RESEARCH PAPER

Development and characterization of a portable electrochemical aptasensor for IsdA protein and *Staphylococcus aureus* detection

Shokoufeh Soleimani[1] · Tracy Ann Bruce-Tagoe[2] · Najeeb Ullah[2] · Meredith G. Rippy[3] · Henry G. Spratt[3] ·
Michael K. Danquah[1,2]

Abstract

Staphylococcus aureus (*S. aureus*) is recognized as one of the most common causes of gastroenteritis worldwide. This pathogen is a major foodborne pathogen that can cause many different types of various infections, from minor skin infections to lethal blood infectious diseases. Iron-regulated surface determinant protein A (IsdA) is an important protein on the *S. aureus* surface. It is responsible for iron scavenging via interaction with hemoglobin, haptoglobin, and hemoglobin-haptoglobin complexes. This study develops a portable aptasensor for IsdA and *S. aureus* detection using aptamer-modified gold nanoparticles (AuNPs) integrated into screen-printed carbon electrodes (SPCEs). The electrode system was made of three parts, including a carbon counter electrode, an AuNPs/carbon working electrode, and a silver reference electrode. The aptamer by Au–S bonding was conjugated on the electrode surface to create the aptasensor platform. Cyclic voltammetry (CV) and electrochemical impedance spectroscopy (EIS) were utilized to investigate the binding interactions between the aptasensor and the IsdA protein. CV studies showed a linear correlation between varying *S. aureus* concentrations within the range of 10^1 to 10^6 CFU/mL, resulting in a limit of detection (LOD) of 0.2 CFU/mL. The results demonstrated strong reproducibility, selectivity, and sensitivity of the aptasensor for enhanced detection of IsdA, along with about 93% performance stability after 30 days. The capability of the aptasensor to directly detect *S. aureus* via the IsdA surface protein binding was further investigated in a food matrix. Overall, the aptasensor device showed the potential for rapid detection of *S. aureus*, serving as a robust approach to developing real-time aptasensors to identify an extensive range of targets of foodborne pathogens and beyond.

Keywords Foodborne pathogen · *Staphylococcus aureus* · Aptasensor · IsdA surface protein · Electrochemical · Aptamer

Introduction

Staphylococcus aureus is a Gram-positive bacterium and, as a foodborne pathogen, is critical in the food industry due to its ubiquity, ability to produce heat-stable toxins, and the rapid commencement of symptoms in affected individuals [1, 2]. Its prevalence in food processing and preparation environments is a persistent threat to food safety [3, 4]. The production of potent enterotoxins by *S. aureus* causes even low levels of contamination [5, 6], and it will be a serious concern as they can lead to severe cases of staphylococcal food poisoning within hours of consumption [7]. The economic impact on the food industry is significant, as outbreaks of *S. aureus*-related foodborne illnesses can result in product recalls, legal liabilities, and damage to brand reputation [8]. Therefore, developing accurate and rapid detection methods is crucial to recognizing and mitigating *S. aureus* contamination in food products and protecting public health and the food industry's interests.

Among the surface proteins of *S. aureus*, IsdA has gained considerable attention due to its crucial role in the pathogenesis of the bacterium [9, 10]. IsdA is involved in host cell adhesion, immune evasion, and iron acquisition, making it

✉ Michael K. Danquah
mdanquah@utk.edu

1 Department of Mechanical, Aerospace, and Biomedical Engineering, University of Tennessee, Knoxville, TN 37996, USA

2 Department of Chemical and Biomolecular Engineering, University of Tennessee, Knoxville, TN 37996, USA

3 Department of Biology, Geology, and Environmental Science, University of Tennessee, Chattanooga, TN 37403, USA

a key virulence factor [11, 12]. Understanding the characteristics and functions of IsdA is essential for clarifying the mechanisms of *S. aureus* pathogenicity and developing targeted theragnostic systems [13]. Detection and identification of *S. aureus* have traditionally depended on culture-based methods, which are time-consuming and require skilled personnel [14]. However, many rapid and sensitive diagnostic tools have recently been developed targeting IsdA [15, 16]. Various techniques, including immunoassays [17], nucleic acid-based methods [18], and mass spectrometry [19], are used to detect IsdA as a specific biomarker of *S. aureus* infection. With these limitations in mind, electrochemical methods have emerged as promising alternatives for detecting *S. aureus* [19, 20]. Electrochemical techniques offer several advantages, such as real-time monitoring, rapid response, high sensitivity, and the potential for miniaturization and portability [21, 22]. These features make electrochemical biosensors well-suited for point-of-care applications, allowing early diagnosis and timely intervention [23, 24].

Among diverse types of electrochemical sensors, SPCEs have become popular as biosensing platforms in electrochemical studies [24, 25] in comparison to other detection methods such as polymerase chain reaction (PCR) [26], recombinase-aided amplification [27], and enzyme-linked immunoassay (ELISA) [28]. While PCR is highly sensitive and specific, it requires DNA extraction and amplification, which can be time-consuming and may not always be suitable for rapid diagnostics. Conversely, ELISA is commonly used for its simplicity but may lack real-time monitoring capabilities [29, 30]. SPCE, as an electrochemical sensor, provides a convincing alternative method due to its rapid response time and portability. This electrode consists of three parts (counter electrode, reference electrode, and working electrode), which allow for precise and controlled electrochemical measurements. Moreover, this method is cost-effective and can be easily functionalized with specific aptamers or biomolecules, enabling selective and accurate identification of *S. aureus*. The discussed versatility makes SPCE-based electrochemical sensors provide a promising framework for rapid, on-site, and precise identification of *S. aureus*, with applications ranging from clinical diagnostics to food safety and environmental monitoring [31, 32].

Aptamers, which are RNA or single-stranded DNA molecules, have emerged as novel biorecognition elements in biosensors. Aptamers present numerous benefits compared to conventional antibodies, featuring high affinity and specificity, enhanced stability, and straightforward synthesis [33–35]. IsdA-specific aptamers can be generated through the Systematic Evolution of Ligands by Exponential Enrichment (SELEX) [36, 37]. Nowadays, nanomaterials are widely used in different fields of science, including sensing. Applying nanotechnology in electrode customization is efficacious in improving electrochemical biosensors' responses [38, 39]. AuNPs have been extensively studied for their unique physicochemical properties, featuring a large surface area, superior conductivity, and biocompatibility. Such attributes render AuNPs ideal for signal enhancement and surface attachment in biosensor applications [40–42]. Functionalizing SPCEs with AuNPs increases the surface area for analyte capturing, leading to improved sensitivity and enhanced detection limits [43, 44].

Detecting *S. aureus* with the help of aptamers and electrochemical methods has been reported in many publications in recent years. In 2022, El-Wekil et al. reported the dual recognition aptasensor for sensing *S. aureus* based on a binary hybrid of Au/Fe_3O_4 in natural products such as apple juice, conduit water, and milk. This molecularly imprinted aptasensor demonstrated a detection limit of 1 CFU/mL across a dynamic range of 10^1–10^7 CFU/mL [45]. Similarly, in 2022, Nguyen et al. developed a sandwich-type electrochemical aptasensor employing SA37 and SA81 aptamer pairs on a screen-printed gold electrode, achieving *S. aureus* detection in buffer and tap water samples spiked with the bacterium, with detection limits of 39 CFU/mL for SA37 and 414 CFU/mL for SA81 within a range of $1.0 \sim 10^9$ CFU/mL [46]. In 2022, Tian et al. reported an aptasensing technology for quantitative analysis of *S. aureus* made from copper-based metal–organic framework and utilizing Cu_2O nanocrystals (ML-Cu_2O@Cu-MOF), which showed detection limits of 2.0 and 1.6 CFU/mL for EIS and DPV methods, respectively, in a range from 10 to 10^8 CFU/mL [47]. Sohouli et al. published a paper in 2021 based on an electrochemical aptasensor modified with gold and nitrogen-doped carbon nano-onions (NCNO) by using SPCE to detect *S. aureus*, achieving a detection threshold of 3 CFU/mL within a 10–10^8 CFU/mL range [48]. Furthermore, in 2022, Zhou et al. described the development of an electrochemical aptasensor modified with Fe_3O_4, capable of detecting *S. aureus* with a remarkably low detection limit of 0.3 CFU/mL in a linear range of $1 \sim 10^8$ CFU/mL in samples of seawater spiked with *S. aureus*, through stepwise signal amplification [49].

In this study, a portable and highly sensitive electrochemical biosensor was developed to detect the IsdA protein as the target biomarker, along with a preliminary focus on identifying *S. aureus*. This biosensor was engineered utilizing SPCEs modified by AuNPs and functionalized with aptamers specific to the IsdA protein. We hypothesized that integrating SPCEs, AuNPs, and aptamers would result in a robust biosensor device with enhanced sensitivity, selectivity, and rapidity for *S. aureus* detection. The resulting biosensor enabled efficient monitoring and quantitative analysis of IsdA in complex biological samples via electrochemical techniques.

Experimental

Materials and reagents

SPCEs enhanced with AuNPs (SPCE/AuNPs) were acquired from Metrohm, USA. Bovine serum albumin (BSA) and protein A (Protein A) were bought from Thermo Fisher, USA. Chemicals such as hydrogen tetrachloroaurate ($HAuCl_4$), sodium phosphate dibasic (Na_2HPO_4), tris–HCl, methanol (CH_3OH), potassium phosphate monobasic (KH_2PO_4), potassium ferricyanide ($K_3[Fe(CN)_6]$), potassium ferrocyanide ($K_4[Fe(CN)_6]$), and 2-mercaptoethanol (2-MCE), along with calcium chloride ($CaCl_2$), magnesium chloride ($MgCl_2$), potassium chloride (KCl), sodium chloride (NaCl), and sulfuric acid (H_2SO_4) were all purchased from Sigma-Aldrich, USA. The crosslinking agents n-hydroxysuccinimide (NHS) and 1-ethyl-3-(3-dimethylaminopropyl) carbodiimide hydrochloride (EDC) were sourced from Cytiva, USA. Additionally, the IsdA-specific aptamer sequence (5′-gcg cac gcg ugu gua gua cac acg auc gcg cgc aca auau-3′), formulated in our lab, was synthesized by Integrated DNA Technologies, USA [50]. Culture media, including tryptic soy broth (TSB) and tryptic soy agar (TSA), were acquired from Becton, Dickinson and Company, located in Maryland, USA. Furthermore, the IsdA protein was sourced from CUSABIO, USA. Double distilled water (DDW) was utilized to prepare all solutions.

Aptasensor fabrication

The SPCE/AuNPs electrode was first activated by 20 μL solution containing 0.4 M EDC/0.1 M NHS (1:1v) for 30 min and then washed with DDW [51, 52]. EDC facilitates the activation of carboxyl groups on AuNPs by generating a reactive O-acylisourea intermediate. This intermediate, however, is inherently unstable in aqueous environments, tending towards hydrolysis, which results in the reformation of carboxyl groups and the liberation of a urea by-product. To enhance the coupling efficiency of the reaction, NHS is introduced. NHS interacts with the EDC-activated carboxyl groups to create a more stable NHS-ester intermediate, which is significantly more resistant to hydrolysis than its O-acylisourea counterpart, thereby exhibiting increased reactivity towards primary amines. Consequently, the NHS-ester modified carboxyl groups on the AuNPs are primed to engage with primary amine groups located on the aptamer, culminating in the formation of durable amide bonds and the release of NHS. This crucial step seamlessly attaches the biomolecule to the AuNPs' surface, ensuring effective bioconjugation

[53, 54]. To conjugate the aptamer onto the surface of the AuNPs-modified electrodes, 5 μM of the aptamer solution was dropped on the SPCE/AuNPs and maintained at the temperature (36 ± 2 °C) for 6 h. Then, binding buffer (100 mM NaCl, 5 mM KCl, 2 mM $MgCl_2$, 20 mM Tris–HCl, and 1 mM $CaCl_2$) was used to rinse the electrode to remove any unbounded aptamer on the electrode surface. Subsequently, to block any remaining active sites on the modified electrode surface, 10 μL of 1 mM 2-MCE solutions was injected on the surface and incubated for 1 h. The electrode was washed with DDW and dried at room temperature [55]. The final electrode (aptasensor) was kept at 4 °C until utilization. Scheme 1 shows a visual representation of the aptasensor preparation steps.

Electrode characterization

Fluorescent characterization was done using the SP8 White Light Laser Confocal System (Germany) by applying a proper filter configuration. Analysis of the SPCE/AuNPs, aptamer, and aptamer/IsdA bonding on the surface was done by adding 20 μL fluorescence dye (6–carboxyfluorescein (FAM)) to the aptasensor surface and maintained at room temperature. In the next step, 20 μL of FAM and 20 μL of 2 μM IsdA were added to the surface of the aptasensor and incubated at room temperature. The samples were coated with foil in a Petri dish to avoid any photoreaction due to the FAM.

Scanning electron microscopy (SEM, Zeiss Dual Beam FIB/SEM, Germany) was used to characterize the bare SPCE/AuNPs' surface to show the distribution of AuNPs on the surface and their average size. The aptasensor surface was also analyzed by SEM to observe the attachment of the aptamer (5 μM) to the AuNPs on the surface of SPCE/AuNPs.

Electrochemical characterization of the aptasensor

The electrochemical experiments were conducted using the μStat-i 400 s potentiostat/galvanostat (Metrohm, USA) at a pH of 7.3 across a potential span from -0.1 to 0.9 V, with a scan rate of 0.05 V/s for CV analysis. The response of the aptasensor assay was elicited using a 5 mM probe solution comprised of ferri-/ferrocyanide ($[Fe(CN)_6]^{-3/-4}$) in conjunction with 0.1 M KCl [56]. KCl helps to keep a constant ionic power, improves the overall conductivity of the solution, facilitates transferring electrons between the redox species in the solution and the working electrode efficiently, and ensures better sensitivity and response in electrochemical measurements [57]. 1 mM NaCl was used to wash bounded IsdA protein on the aptasensor surface, followed by DDW rinsing. All analytical measurements were repeated three times, and an average curve was used.

Scheme 1 Overview of the aptasensor fabrication process for IsdA protein and *S. aureus* bacteria detection
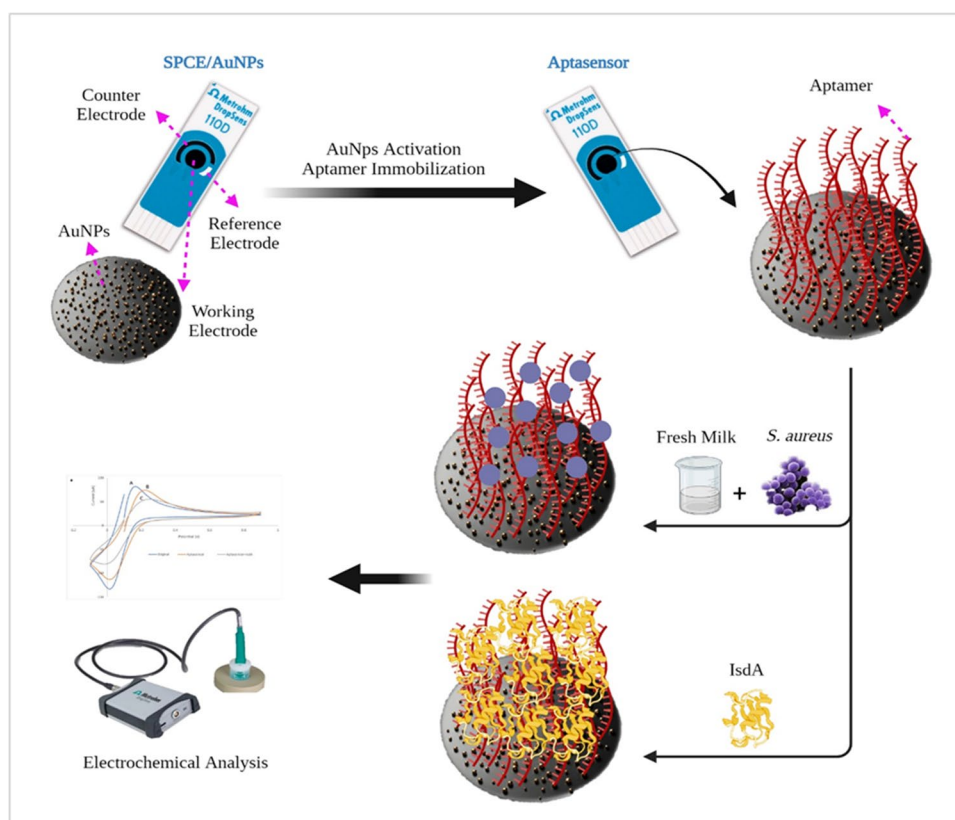
Aptasensor reproducibility analysis

The reproducibility of the aptasensor as the recognition element is critically important for ensuring its reliability for real biosensing applications. Reproducible results are essential for confirming the accuracy of the aptasensing measurements. Consistent readings across multiple tests and conditions validate the reliability of the aptasensor for detecting specific targets, ensuring that data generated are dependable and can be used for making informed decisions. This process was done by fabricating five different aptasensors using the same fabricating method and laboratory conditions previously described. CV curves were taken in a pH of 7.3 in a 5 mM probe solution ($[Fe (CN)_6]^{-3/-4}$, 0.1 M KCl) to detect 2 μM IsdA.

Aptasensor stability analysis

The stability analysis determines the long-term usability, reliability, and performance of the aptasensor in real-world applications, ensuring that the aptasensor can consistently detect its target with high accuracy and specificity over time under various storage and operational conditions. This is essential for practical applications, such as food safety and environmental monitoring, where dependable and durable sensors are needed. Furthermore, understanding the stability

of the aptasensor helps optimize storage conditions, extend shelf life, and reduce costs, making the technology more accessible and commercially viable. To determine the stability of the aptasensor, a freshly fabricated aptasensor was stored at 4 °C for a duration of 30 days. CV measurements were done on the first day, 2nd day, 8th day, 16th day, 25th day, and 30th day of the storage period to detect 2 μM IsdA. The CV measurements were taken in contact with a 5 mM probe solution at a pH of 7.3. After every analysis, the aptasensor was washed with 1 mM NaCl and DDW, dried at room temperature, and stored in the fridge for the next test.

Aptasensor selectivity analysis

This characteristic is fundamental for the accuracy and reliability of the aptasensor in practical environments, where the presence of closely related compounds could lead to false results. In this work, we tested the selectivity of the aptasensor in the presence of BSA and protein A. Differential pulse voltammetry (DPV) and CV were used for the selectivity analysis of the aptasensor due to its enhanced sensitivity, better resolution, and lower background current. DPV improves the signal-to-noise ratio by applying a series of pulses on top of a linear potential sweep, allowing for the detection of smaller current changes due to redox reactions of the analyte. This heightened sensitivity makes DPV

suitable for detecting even low concentrations of analytes [58, 59]. Consequently, DPVs of aptasensor were taken in a 5 mM probe solution with a pH of 7.3 without any agent. The sensor was washed, and DPV and CV measurements were taken for the unbound aptasensor and after BSA and protein A (5 μM) binding in the presence of 5 mM probe solution at pH 7.3. IsdA protein binding to the aptasensor surface in the presence of BSA and protein A was analyzed via DPV and CV measurements using 5 μM IsdA in the probe solution (pH 7.3). After that, the sensor was washed with 1 mM NaCl and DDW.

Aptasensor regeneration analysis

To evaluate the reusability of the aptasensor and ensure consistent performance across multiple cycles of analyte detection, a regeneration analysis was carried out to assess the consistency of the aptasensor after several applications. For this purpose, a single aptasensor device was used during the study. First, the aptasensor response to IsdA detection in 5 mM probe solution and pH 7.3 was recorded. Then, the aptasensor was washed with 1 mM NaCl and DDW, and CV curves were measured in a 5 mM probe solution of pH 7.3 without IsdA. The process was repeated with the same aptasensor five times sequentially in the following steps.

S. aureus culture preparation

The preparation of *S. aureus* cultures for detection analysis was conducted in the Clinical Infectious Disease Control (CIDC) research lab at the University of Tennessee at Chattanooga. A lab strain of *S. aureus* (traceable to ATCC strain 25,923) was procured from the UTC Microbiology culture collection and sustained within the CIDC research laboratory at UTC on either TSA slants or in TSB. The study also required 0.85% sterile saline and TSB for subsequent serial dilutions of the *S. aureus*.

TSA was used to grow the *S. aureus* cultures and plate them for initial enumeration via a viable plate count in the creation of a calibration curve relating optical density at 600 nM (OD600) to colony forming units per milliliter (CFU/mL). TSA and TSB were made according to the manufacturer's instructions and autoclaved for 20 min before pouring into sterile Petri dishes or used for the detection analysis at 15 psi. The TSA slants were made by transferring aliquots of the boiled and mixed liquid TSA to test tubes in an autoclave prior to sterilization (Primus Sterilizer Co LLC, USA). The TSA plates were stacked and dehydrated for 72 h at room temperature before being utilized. For dilutions, sterile saline (0.85% NaCl) was formulated by dissolving 8.5 g of NaCl in 1 L of DDW before sterilization in the autoclave.

Food matrix sample preparation

Milk was selected as the food matrix to test the capacity of the aptasensor to detect *S. aureus* in real samples. To maintain the electrochemical environment, the probe solution was added to the milk sample, followed by 1 CFU *S. aureus* to simulate a contamination scenario. The sample was not incubated and was immediately processed for analysis to assess the presence of *S. aureus* via EIS and CV (potential range from − 0.1 V to 1 V and scan rate of 0.05 V/s) measurements.

S. aureus calibration test method

To produce six different concentrations of *S. aureus*, the *S. aureus* was grown on a TSA plate for approximately 48 h at 37 °C, and an overnight culture of *S. aureus* in TSB was made. After 48 h, one isolated colony of *S. aureus* was taken from the TSA plate using a sterilized inoculating loop and added to 10 mL of sterile TSB. This liquid culture was mixed by vortexing for 15 s to warrant thorough mixing of the *S. aureus* cells within the media. *S. aureus* and TSB mixture was then shaken at 180 rpm for 16 h at 37 °C. At the 16th hour, 1 mL of the mixture was pipetted into a cuvette, and an absorbance reading was measured at 600 nM using a Fisher Scientific Spectro Master 415 spectrophotometer. Using a previously constructed calibration curve relating OD600 of this strain of *S. aureus* to CFU/mL, the culture was diluted with sterile TSB to an absorbance of 0.437 to estimate the number of cells in the overnight culture as 1.029×10^8 cells. One hundred microliters of the overnight culture was then transferred from this tube into a sterile test tube with 9.9 mL of sterile 0.85% NaCl saline. This mixture was vortexed for 15 s, and then 1 mL of the mixture was relocated to a tube consisting of 9 mL of sterile 0.85% NaCl saline. This was repeated four additional times, with each tube being vortexed for 15 s and immediately placed in an ice bath to avoid further growth of the bacteria. The serial dilution was implemented to have six vials of *S. aureus* with different concentrations. The estimated number of cells in the dilutions was determined using the calibration curve.

Results and discussion

Aptasensor characterization

Fluorescent and SEM imaging techniques are essential techniques utilized for aptasensor characterization. A fluorescent microscope illuminates the sample with a specific wavelength of light, causing fluorescently labeled components to emit light at a different wavelength, which is then detected to form an image [60]. Figure 1A, part I, functioned as the
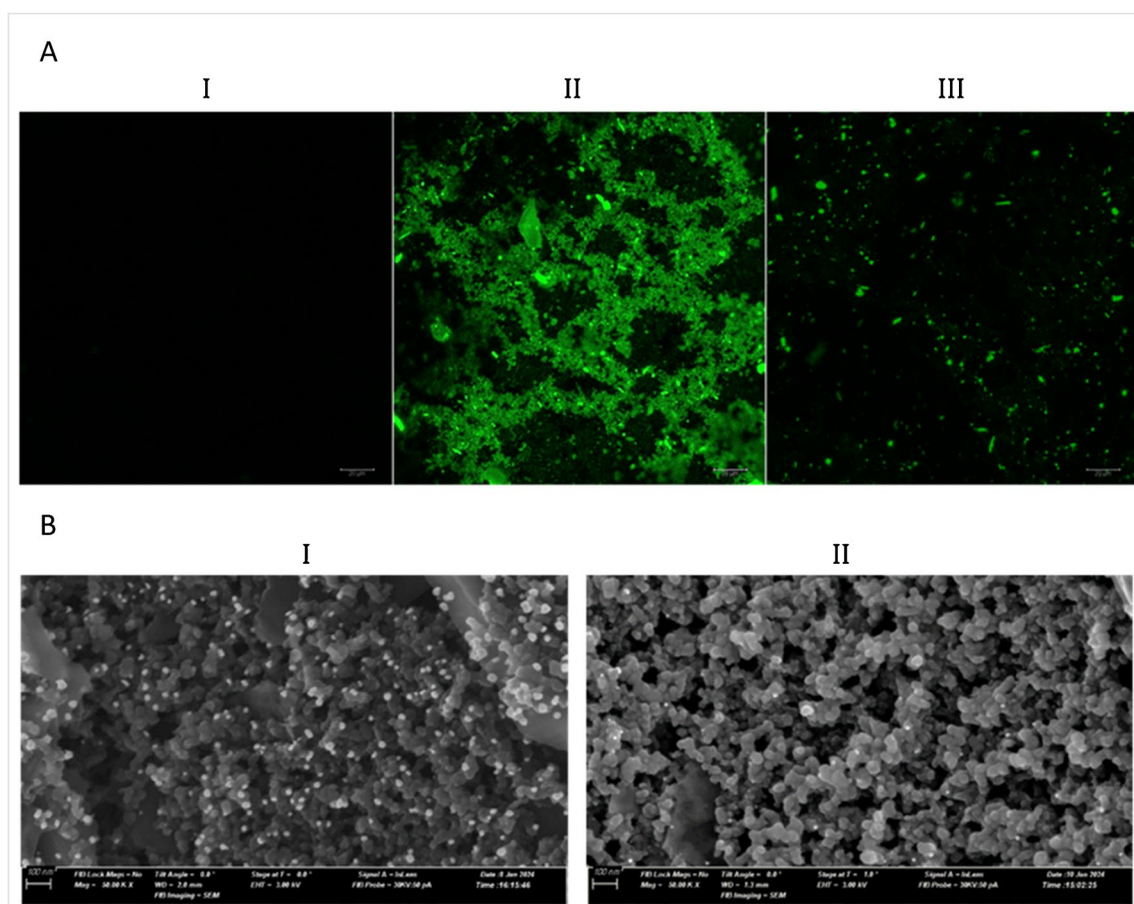
Fig. 1 Fluorescence (**A**) and SEM images (**B**) of (I) bare SPCE/AuNPs, (II) aptasensor, and (III) aptasensor in presence of 2 μM IsdA

negative control, confirming the absence of fluorescently tagged components. In Fig. 1A, part II, FAM was applied to the aptasensor. The observed luminous, amorphous fluorescence signals substantiated the successful immobilization of fluorescently tagged aptamers on the substrate, while the detection of bright green spots suggested residual free dye on the substrate, attributable to the absence of a post-incubation rinse. Moreover, Fig. 1A, part III, illustrated the fluorescence quenching upon the target molecule (IsdA) binding to the aptamer, indicating efficient energy transfer from the excited FAM to IsdA, reflecting optimal aptamer immobilization and robust binding affinity with IsdA [42].

SEM imaging operates by scanning a focused beam of electrons across a sample, where the electrons interact with the atoms in the sample to produce various signals that can be detected to form a high-resolution image [61]. Figure 1B, part I, shows the morphology of the bare SPCE/AuNPs by SEM without any modification on the surface. The uniform distribution and homogeneity of the AuNPs, approximately 25 nm in size, set against the darker matrix of the printed carbon electrode. This arrangement facilitated the effective immobilization of the aptamer on the surface of the SPCE/

AuNPs to create a more sensitive aptasensor. In Fig. 1B, part II, increased surface coverage on the nanoparticles compared to the unmodified surfaces observed in part I, proves that an additional molecular layer (aptamers) has been attached. This is further supported by changes in texture and contrast on the gold nanoparticles; after the addition of aptamers, the nanoparticles exhibit a less smooth, more granular appearance, which is indicative of aptamer binding to the metallic surface. The uniformity in the appearance of these changes across multiple nanoparticles implies a systematic modification rather than random contamination, reinforcing the conclusion that aptamers are consistently bound across the surface. These visual indicators in the SEM image provide qualitative evidence of successful aptamer immobilization, which is facilitated by the strong affinity between thiol groups in the aptamers and the gold surface. This affinity leads to the formation of stable covalent bonds via gold-thiolate interactions, ensuring robust and oriented attachment of the aptamer molecules. This immobilization is crucial for enhancing the sensor's performance, as it ensures that the aptamers maintain their structural integrity and functional orientation, thus optimizing their interaction with target

molecules. Robust attachment of aptamers to the AuNPs facilitates rapid and efficient target capture, which is essential for the real-time detection capabilities of the aptasensor [62, 63].

The choice of EDC/NHS chemistry was driven by its effectiveness in creating stable amide bonds between the carboxyl groups on the activated electrode surface and the amine groups present on the aptamer [64, 65]. This covalent bonding ensures a strong and stable attachment of the aptamer [66], minimizing the risk of desorption under assay conditions and thus enhancing the sensitivity and specificity of the aptasensor [67]. The EDC/NHS approach provides several advantages, including a controlled orientation of the aptamer on the sensor surface, which is critical for maintaining the binding affinity and specificity of the

aptamer towards the target IsdA protein of *S. aureus*. The use of EDC/NHS chemistry in our design facilitates a denser and more uniform aptamer coating, contributing to a larger active surface area for target interaction and improved performance [64].

CV and EIS measurements

Within the theoretical framework, variations in the voltammetric peak current observed in CV curves throughout the electrode modification process are attributed to alterations in charge transfer resistance. Figure 2 displays the CV and EIS curves corresponding to the steps in the electrode modification process. The CV and EIS profiles for the unmodified SPCE/AuNPs in the $[Fe\,(CN)_6]^{-3/-4}$ in 0.1 M KCl solution

Fig. 2 **a** CVs and **b** EISs of different electrodes in contact with 5 mM ($[Fe\,(CN)_6]^{-3/-4}$, 0.1 M KCl) in pH of 7.3, where curve (A) is the bare SPEC/AuNPs, curve (B) is aptasensor, and curve (C) shows the aptasensor and IsdA (2 µM) interaction response
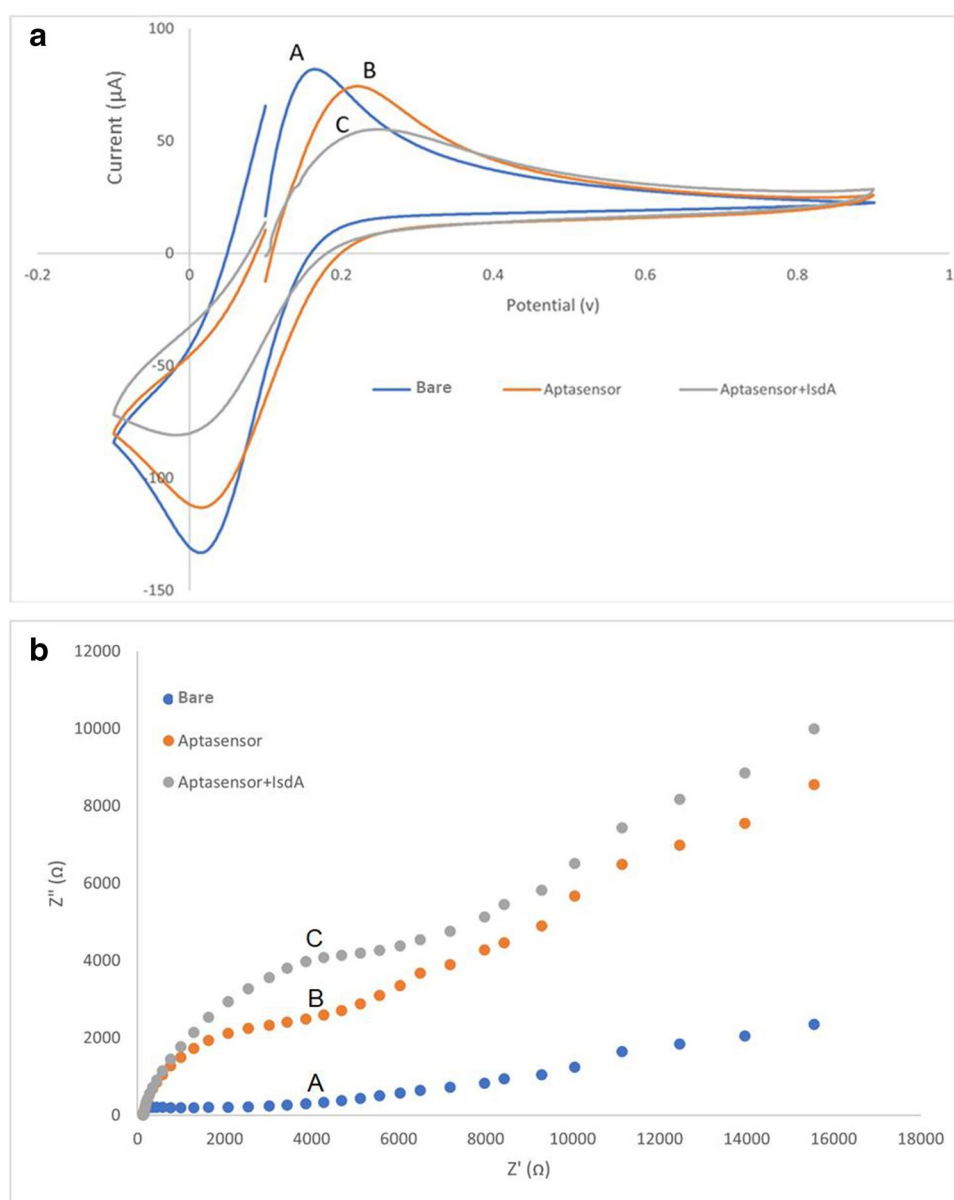
(curve a) served as a baseline for comparing the CV and EIS responses across the different stages of immobilization. The attachment of the aptamer to the SPCE/AuNPs electrode led to a noticeable reduction in current and an elevation in resistance (curve b) during the oxidation and reduction of [Fe $(CN_{)6}]^{-3/-4}$, signifying a decrease in electron transfer from the SPCE/AuNPs surface to the [Fe $(CN)_6]^{-3/-4}$ solution. Adding 2 μM IsdA to the aptasensor surface (curve c) further reduces the current in CV and increases the resistance in EIS, indicating an obstructive effect of IsdA to electron transfer at the electrode surface, a phenomenon that arises from the formation of the IsdA-aptamer complex. Therefore, the extent of variation in the electron transfer resistance at the electrode/solution interface during [Fe $(CN)_6]^{-3/-4}$ oxidation/reduction acts as the underlying mechanism for detection. These observations indicate that the presence of aptamers restricts the electron flow on the electrode surface, consequently reducing the overall efficiency of electron transfer in the system, which proves that aptamer and protein active sites have not been compromised [68, 69].

At the molecular or atomic level, the inhibitory effect of IsdA-aptamer complex formation on electron transfer can be attributed to several key factors. When the IsdA protein binds to the aptamer at the relevant binding sites, it forms a complex through non-covalent interactions [16, 70]. This complexation disrupts the electrochemical process. The physical presence of the IsdA-aptamer complex blocks the electrode's active sites where the redox reaction is supposed to occur, effectively shielding the electrode surface from the analyte or redox species. Moreover, binding of IsdA to the aptamer can lead to conformational changes in the aptamer's structure, which may alter its orientation on the electrode, making it less conducive for electron transfer. Additionally, the complexation may cause electronic interactions that modify the energy levels of the redox species, impeding their ability to participate in electron transfer reactions. Electron transfer kinetics can also be hindered as the complex formation introduces kinetic barriers requiring dissociation or structural rearrangements before electron transfer can occur [71, 72].

Analysis of aptasensor application, reproducibility, stability, selectivity, and regeneration

The preparation and detection times of the aptasensor show its advantages/applicability. The preparation process of the aptasensor, which includes sensor activation, incubation for covalent bond formation, and aptamer immobilization, spans ~ 7.5 h, which is equal to or less than other reported studies in Table 1. This ensures the aptasensor is primed for optimal performance and specificity towards the IsdA protein of *S. aureus*. The aptasensor demonstrates a rapid detection time of ~ 1 min using direct *S. aureus* with no sample preparation, highlighting its efficiency and rapid nature. This rapid detection time shows the potential for real-time applications and its suitability for scenarios requiring quick pathogen monitoring and assessment.

Figure 3 shows that the CV data from five independently fabricated electrodes were remarkably consistent, demonstrating minimal variation in their electrochemical responses. This uniformity shows the reproducibility of aptasensors and the reliability of our fabrication process. As shown in Fig. 4, stability response signals retained 93% of their initial strength for 2 μM IsdA detection after a storage period of 30 days at 4 °C, proving the aptasensor performance stability over an extended period. Such a finding is important to determine the potential of the aptasensor for extended use. The DPV and CV curves of the aptasensor's selectivity analysis (Fig. 5) showed a stronger response in detecting IsdA in comparison to the BSA and protein A. The aptamer and IsdA showed a stronger binding affinity, generating a stable complex that hinders access to electrons on the sensor surface. As a consequence, the current response is reduced, leading to a lower peak in the DPV and CV analysis. The BSA and protein A curves show a weaker binding with the aptamer, potentially resulting from non-specific

Table 1 Comparison of different aptasensors in detecting *S. aureus*

| Biosensor	Method	Linear range	LOD	Ref
Pair-based aptamer (SA37, SA81)	CA	1.0 ~ 10^9 CFU/mL	SA37 = 39 CFU/mL SA81 = 414 CFU/mL	[46]
Aptamer/Au/NCNO	EIS	10–10^8 CFU/mL	3 CFU/mL	[48]
Aptamer/ML-Cu$_2$O@Cu-MOF	EIS DPV	10–10^8 CFU/mL	2.0 CFU/mL 1.6 CFU/mL	[47]
Aptamer/Au/Fe$_3$O$_4$	DPV	10–10^7 CFU/mL	1 CFU/mL	[45]
Aptamer/Fe$_3$O$_4$	FSCV	1 ~ 10^8 CFU/mL	0.3 CFU/mL	[49]
Aptamer/SPCE/AuNPs	CV	10–10^6 CFU/mL	0.2 CFU/mL	Current study
Dual-mode ratiometric aptasensor/AuNPs	DPV/ECL	5–10^8 CFU/mL	0.1 CFU/mL	[35]

Fig. 3 Reproducibility CVs of five different aptasensors with the same fabrication process in the presence of 2 μM IsdA in contact with 5 mM ([Fe (CN)$_6$] $^{-3/-4}$, 0.1 M KCl) in pH of 7.3
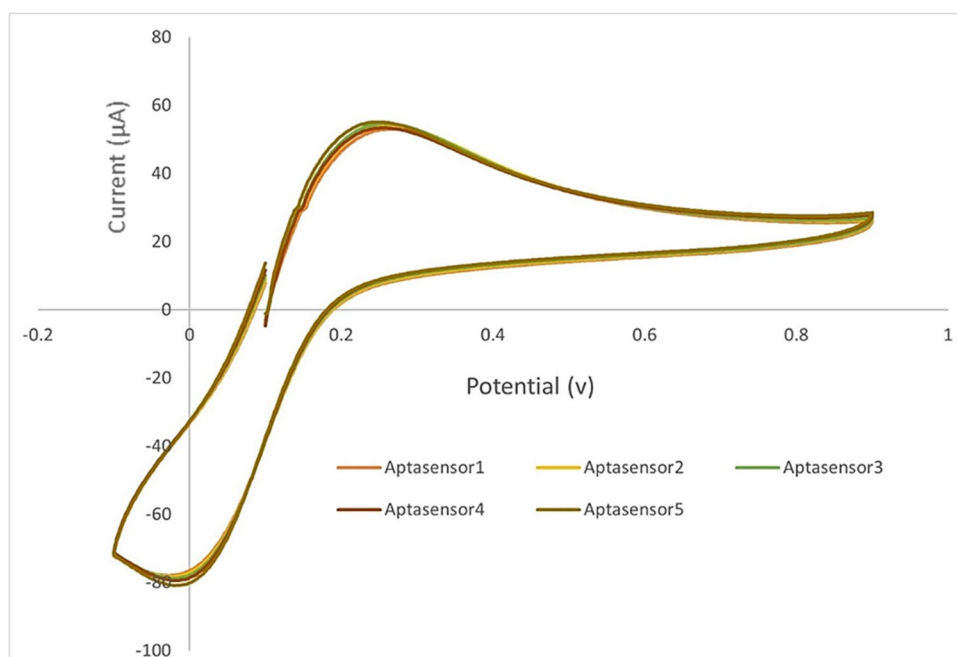
Fig. 4 CVs of aptasensor's stability in detecting 2 μM IsdA during 30 days in contact with 5 mM ([Fe (CN)$_6$] $^{-3/-4}$, 0.1 M KCl) in pH of 7.3
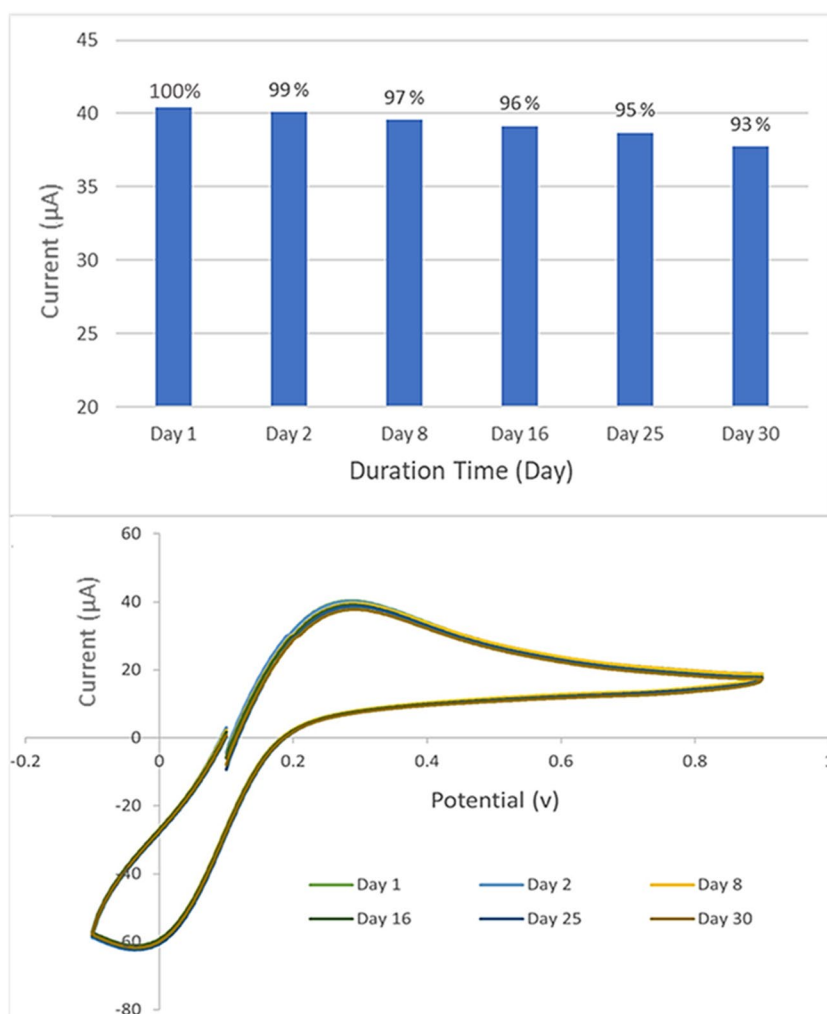
Fig. 5 DPV (**A**) and CV (**B**) selectivity analysis of the aptasensor using BSA (5 μM), protein A (5 μM), and IsdA (5 μM) in the presence of 5 mM ([Fe (CN)$_6$] $^{-3/-4}$, 0.1 M KCl) at pH 7.3
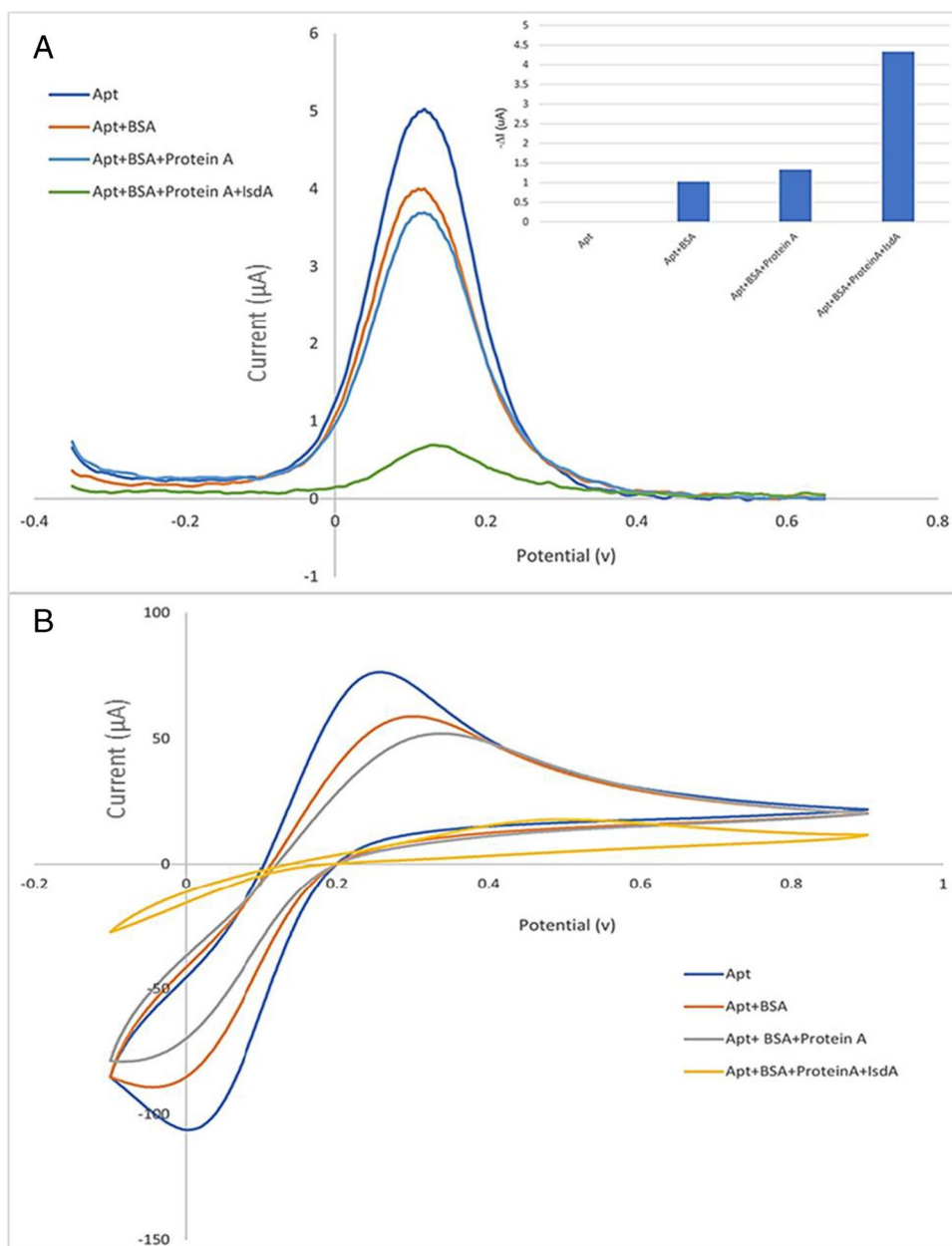

interactions. Non-specific binding is commonly observed between aptamers and non-targets [73, 74].

CV data presented in Fig. 6 indicates that the aptasensor retains its functionality after multiple washing steps. The persistence of the peak currents through several cycles of washing and binding to IsdA suggests a stable attachment of the aptamer to the sensor surface. It is also notable that the peak currents do not exhibit significant degradation in intensity after each washing, implying that the binding of IsdA to the aptamer does not deteriorate the performance of the aptasensor. The ability of the aptasensor to maintain consistent electrochemical signals after repeated exposure to the analyte and subsequent washings is a strong indicator of its

reusability. This characteristic is particularly important for practical applications where the durability of the aptasensor and its regeneration ability are key factors for cost-effective and sustainable monitoring.

Food matrix analysis

The results from the CV and EIS analyses of the capability of the aptasensor to detect *S. aureus* in the milk are presented in Fig. 7. Figure 7 (I) shows the CV curves for the aptasensor without *S. aureus* (curve A) and the presence of *S. aureus* in milk (curve B). The CV curve of the unbound aptasensor shows well-defined redox peaks. The peak currents are
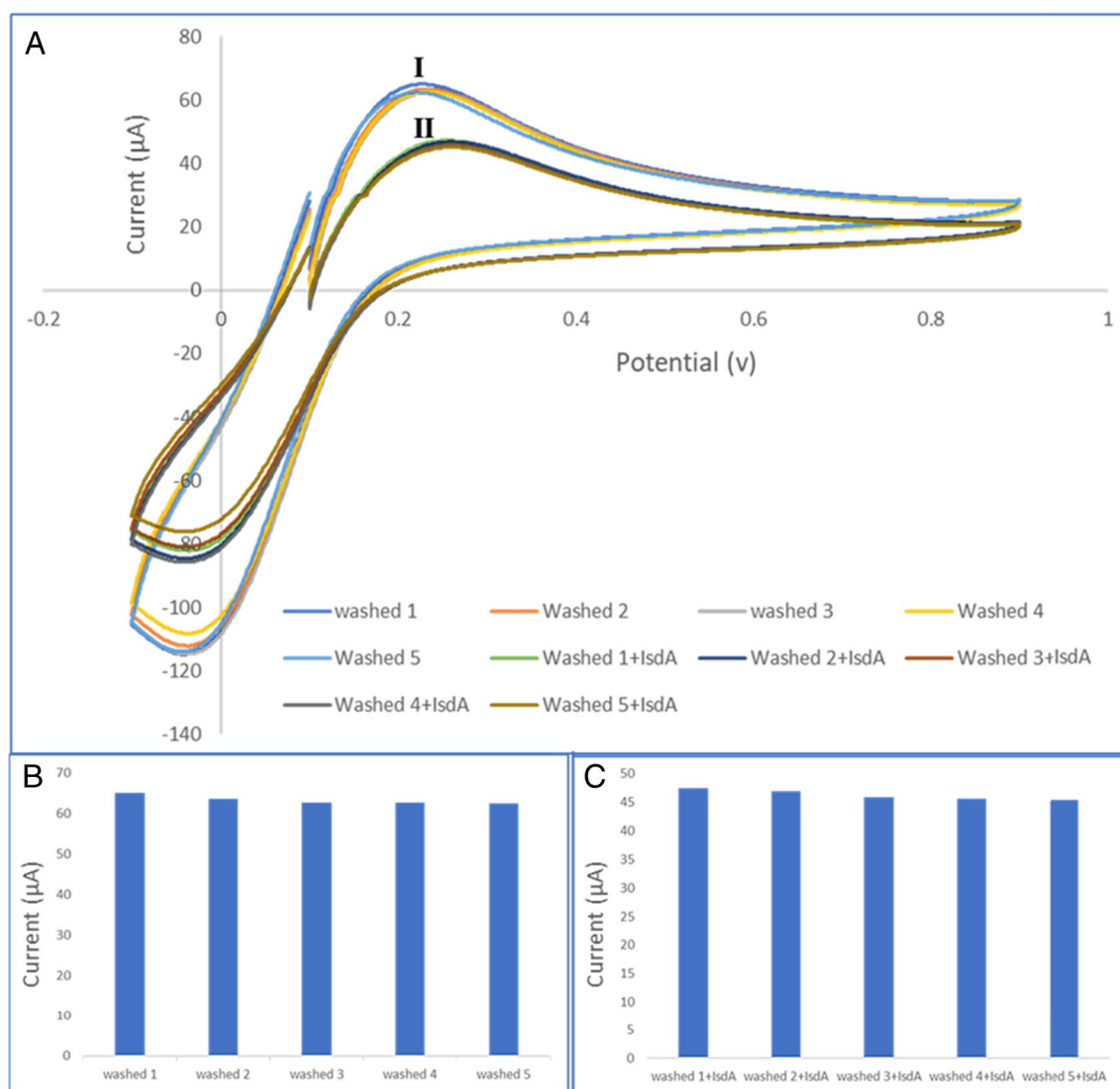
Fig. 6 Regeneration characteristics of the aptasensor: **A** CV curves after washing the aptasensor+IsdA (I) with 1 mM NaCl and DDW in contact with 5 mM ([Fe $(CN)_6$] $^{-3/-4}$,0.1 M KCl) in pH of 7.3 and (II) CV curves of aptasensor after adding IsdA (2 µM) in contact with 5 mM ([Fe $(CN)_6$].$^{-3/-4}$,0.1 M KCl) in pH of 7.3, **B** bar chart of (I), and **C** bar chart of (II)

higher, indicating efficient electron transfer between the electrode surface and the electrolyte. Upon interaction with the milk sample contacting *S. aureus*, the CV curve shows a noticeable decrease in peak currents. This decrease is attributed to the binding of *S. aureus* to the aptasensor, which hinders electron transfer and reduces the overall current. The reduction in peak current is indicative of the successful capture and detection of *S. aureus* by the aptasensor to the milk matrix. The significant change in the CV profile shows that the aptasensor effectively interacts with the bacteria, leading to measurable electrochemical changes. This confirms the aptasensor's sensitivity and specificity towards *S. aureus* detection in food samples such as milk. Figure 7 (II) shows the EIS measurements of the aptasensor without *S.*

aureus (curve A) and with *S. aureus* in milk (curve B). The plots display the imaginary component of impedance (-Z) against the real component of impedance (Z). The Nyquist plot for the bare aptasensor exhibits a large semicircular arc, indicating high charge transfer resistance (R_ct). The large diameter of the semicircle suggests that the aptasensor surface has a high electron transfer resistance when not bound to any target. The presence of *S. aureus* in milk causes a significant reduction in the semicircular arc's diameter. This reduction in R_ct implies that the binding of *S. aureus* to the aptasensor decreases the electron transfer resistance, likely due to the formation of a conductive biofilm or changes in the surface charge distribution upon binding. The EIS data further supports the CV findings, demonstrating that the

Fig. 7 CV (I) and EIS (II) curves of the aptasensor in milk samples containing 1 CFU *S. aureus* in the presence of 5 mM ([Fe (CN)$_6$] $^{-3/-4}$, 0.1 M KCl) at pH 7.3
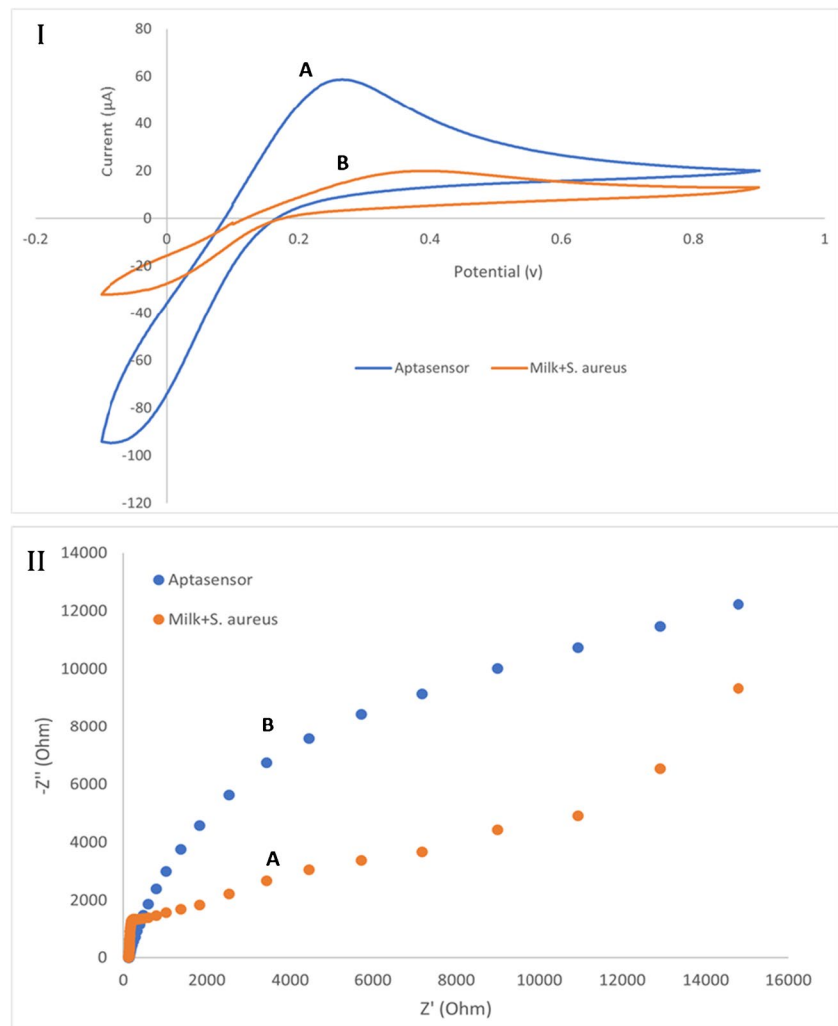

presence of *S. aureus* contaminated milk on the aptasensor surface significantly alters the electrochemical properties of the sensor. The decrease in impedance upon *S. aureus* binding indicates a successful interaction between the aptasensor and the bacteria, confirming the sensor's capability to detect low CFUs of *S. aureus* in milk. The combined results from CV and EIS analyses demonstrate the effectiveness of the designed aptasensor in detecting *S. aureus* in milk samples. These findings indicate the potential of the aptasensor for rapid and accurate detection of *S. aureus* in complex food samples.

Analysis of aptasensor detection limit in *S. aureus*

In this study, we evaluated the performance of the aptasensor for pathogen detection using live *S. aureus* samples at different concentrations. CV analysis indicated that the designed aptasensor demonstrated a reliable response for living samples, as expected. Increasing the *S. aureus* concentration resulted in a decrease in the CV curves due

to the increasing aptasensor electrode surface area occupied by the bacteria, which caused a reduction in electron accessibility to the surface of the aptasensor (Fig. 8). The binding between the aptamer and IsdA on the surface of *S. aureus* is highly specific due to the bioaffinity of their structures. Electrostatic interactions, hydrogen bonds, and van der Waals forces contribute to this specificity, forming strong bonds at the binding interface. Moreover, aptamers may undergo conformational changes upon binding. This alteration of the aptamer's structure is essential for achieving a tight bond with IsdA and a stable complex [48, 72]. If the *S. aureus* concentration increases, more binding sites on the aptasensor will become occupied by bacteria, leading to a lower peak in CV curves. However, there is a point at which the available binding sites become saturated, and further increases in cell concentration might not significantly affect the signal, and the sensor will not be sensitive towards the target anymore. On the other hand, if *S. aureus* concentration decreases more than 10 CFU, gradually the CV current peak will reach the peak current
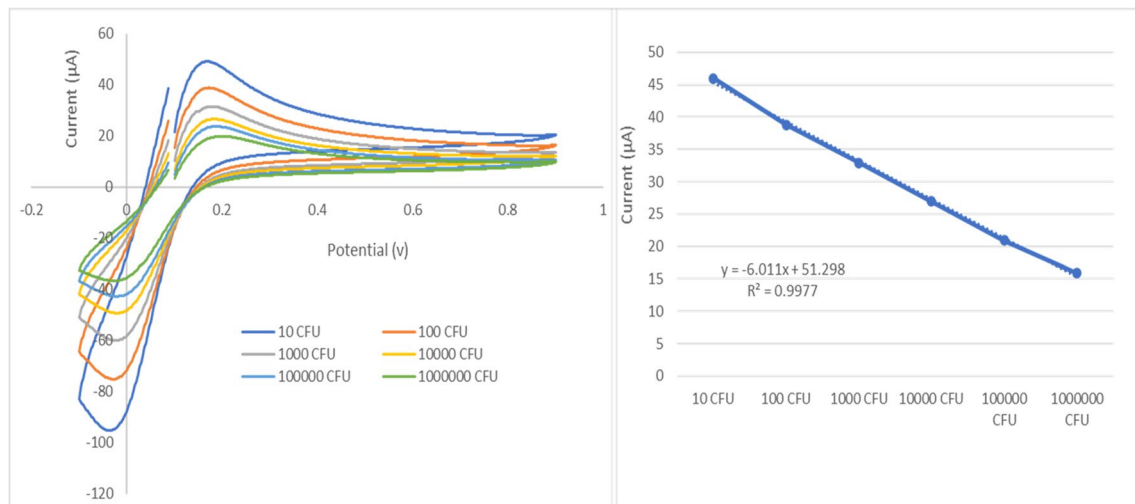
Fig. 8 CVs of the aptasensor in detecting *S. aureus* in 6 different dilutions using 5 mM ([Fe (CN)$_6$] $^{-3/-4}$,0.1 M KCl) for analyzing LOD in pH of 7.3

of 5 mM ([Fe (CN)$_6$] $^{-3/-4}$,0.1 M KCl) without IsdA or *S. aureus* [47, 48].

To identify the aptasensor LOD in detecting *S. aureus*, CV analysis was conducted at a pH of 7.3, employing a potential window from −0.1 to 0.9 V and a scan rate of 0.05 V/s to record peak currents across various *S. aureus* concentrations. Figure 6 illustrates the relationship between peak current intensity and *S. aureus* concentrations, revealing a strong linear relationship within the range of 10 to 10^6 CFU/mL. Furthermore, the LOD and the limit of quantification (LOQ) were determined using Eqs. 1 and 2, respectively. The LOD represents the minimal concentration that can be reliably detected, calculated from the standard deviation of blank measurements (σ) and the absolute slope (|s|) of the calibration plot. A lower LOD signifies enhanced detection capabilities for minimal concentrations of the analyte. Equation 2 calculates the LOQ, indicating the minimal concentration at which the analyte can not only be detected but also quantified with acceptable precision based on σ and |s|. A lower LOQ indicates superior quantification accuracy at low analyte levels. This measure is vital for applications necessitating both detection and precise quantification of low analyte concentrations. The methodology outlined here offers significant potential for sensitive detection of *S. aureus*, showcasing the aptasensor's capability for high-sensitivity applications [75, 76].

$$LOD = \frac{3\sigma}{|s|} \tag{1}$$

$$LOQ = \frac{10\sigma}{|s|} \tag{2}$$

The real innovation of our work lies in the specific combination of the IsdA-binding aptamer and SPCE/AuNPs for the detection of *S. aureus* and achieving an enhanced performance with an LOD of 0.2 CFU and LOQ of 0.66. This is a significant leap in the development of aptasensors for *S. aureus* detection in the context of food safety. The achieved LOD and LOQ represent an enhancement in sensitivity and specificity, setting a new benchmark for *S. aureus* detection approaches. This shows the potential of the aptasensor to offer a rapid and straightforward alternative for the detection of the pathogen while being portable.

Table 1 compares LOD for SPCE/AuNPs aptasensors fabricated in this study with other aptasensors reported in the literature. The results indicate the promising performance of the SPCE/AuNPs aptasensor, demonstrating comparable or better performance characteristics than the other biosensors in the table.

Conclusion

In this study, we successfully developed a robust electrochemical aptasensor for detecting the IsdA surface protein of *S. aureus*. The specificity of the aptasensor, coupled with the combination of SPCE/AuNPs, provides a unique approach for electrochemical signal enhancement, which directly contributes to the enhanced detection performance. The designed aptasensor involved immobilizing the aptamer onto an SPCE modified with AuNPs. By employing CV, electron transfer changes that occurred during the construction and application of the aptasensor were monitored. The aptasensor provided a linear detection range spanning from 10 to 10^6 CFU, with a LOD of 0.2 CFU/mL for *S. aureus*.

The aptasensor demonstrated reproducibility, regeneration capabilities, selectivity, and long-term performance stability. The performance of the aptasensor in food matrix sample shows its potential as a valuable screening tool for the detection of *S. aureus* and its application in food safety monitoring as well as infectious disease monitoring. However, more research validation is needed to support the widespread application of aptasensor technology.

Author contribution Shokoufeh Soleimani: Investigation, writing original draft, data curation, formal analysis. Najeeb Ullah: Methodology, review and editing. Tracy Ann Bruce-Tagoe: Methodology, review and editing. Meredith G. Rippy: Data curation, bacterial investigation. Henry G. Spratt: Methodology, review and editing. Michael K. Danquah: Conceptualization, methodology, validation, supervision, funding acquisition, visualization, project administration, resources, review and editing.

Declarations

Conflict of interest The authors declare no competing interests.

References

1. Narayan KG, Sinha DK, Singh DK. Staphylococcus aureus. In: Narayan KG, Sinha DK, Singh DK, editors. Veterinary Public Health & Epidemiology: Veterinary Public Health- Epidemiology-Zoonosis-One Health. Singapore: Springer Nature Singapore; 2023. p. 301–8. https://doi.org/10.1007/978-981-19-7800-5_32.

2. Algammal AM, Hetta HF, Elkelish A, Alkhalifah DHH, Hozzein WN, Batiha GES, et al. Methicillin-resistant staphylococcus aureus (MRSA): one health perspective approach to the bacterium epidemiology, virulence factors, antibiotic-resistance, and zoonotic impact. Infect Drug Resist. 2020;13:3255–65. https://doi.org/10.2147/IDR.S272733.

3. Schelin J, Wallin-Carlquist N, Thorup Cohn M, Lindqvist R, Barker GC. The formation of Staphylococcus aureus enterotoxin in food environments and advances in risk assessment. Virulence. 2011;2(6):580–92.

4. Castro A, Santos C, Meireles H, Silva J, Teixeira P. Food handlers as potential sources of dissemination of virulent strains of Staphylococcus aureus in the community. J Infect Public Health. 2016;9(2):153–60.

5. Bhatia A, Zahoor S. Staphylococcus aureus enterotoxins: a review. J Clin Diagn Res. 2007;1(3):188–97.

6. Liu D. Enterotoxin-producing Staphylococcus aureus. Molecular Medical Microbiology: Elsevier; 2015. p. 979–95.

7. Do Carmo LS, Cummings C, Roberto Linardi V, Souza Dias R, Maria De Souza J, De Sena MJ, et al. A case study of a massive staphylococcal food poisoning incident. Foodbourne Pathog Dis. 2004;1(4):241–6.

8. Todd EC. Legal liability and its economic impact on the food industry. J Food Prot. 1987;50(12):1048–57.

9. Tiedemann MT, Heinrichs DE, Stillman MJ. Multiprotein heme shuttle pathway in Staphylococcus aureus: iron-regulated surface determinant cog-wheel kinetics. J Am Chem Soc. 2012;134(40):16578–85.

10. Schneewind O, Missiakas D. Sortases, surface proteins, and their roles in Staphylococcus aureus disease and vaccine development. Microbiol Spectr. 2019;7(1):https://doi.org/10.1128/microbiolspec.psib-0004-2018.

11. Clarke SR, Mohamed R, Bian L, Routh AF, Kokai-Kun JF, Mond JJ, et al. The *Staphylococcus aureus* surface protein IsdA mediates resistance to innate defenses of human skin. Cell Host Microbe. 2007;1(3):199–212.

12. Sheldon JR. Iron acquisition mechanisms and their role in *staphylococcus aureus* survival and virulence (Order No. 29243378). Available from ProQuest Dissertations & Theses Global. (2701132606). 2015. Retrieved from https://utk.idm.oclc.org/login?url=https://www.proquest.com/dissertations-theses/iron-acquisition-mechanisms-their-role-i/docview/2701132606/se-2

13. Drury SL, Miller AR, Laut CL, Walter AB, Bennett MR, Su M, et al. Simultaneous exposure to intracellular and extracellular photosensitizers for the treatment of Staphylococcus aureus infections. Antimicrob Agents Chemother. 2021;65(12). https://doi.org/10.1128/aac.00919-21.

14. Sandel MK, McKillip JL. Virulence and recovery of Staphylococcus aureus relevant to the food industry using improvements on traditional approaches. Food Control. 2004;15(1):5–10.

15. Toley BJ, Covelli I, Belousov Y, Ramachandran S, Kline E, Scarr N, et al. Isothermal strand displacement amplification (iSDA): a rapid and sensitive method of nucleic acid amplification for point-of-care diagnosis. Analyst. 2015;140(22):7540–9.

16. Wijesinghe KM, Sabbih G, Algama CH, Syed R, Danquah MK, Dhakal S. FRET-based single-molecule detection of pathogen protein isdA using computationally selected aptamers. Anal Chem. 2023;95(26):9839–46. https://doi.org/10.1021/acs.analchem.3c00717.

17. Wiriyachaiporn S, Howarth PH, Bruce KD, Dailey LA. Evaluation of a rapid lateral flow immunoassay for Staphylococcus aureus detection in respiratory samples. Diagn Microbiol Infect Dis. 2013;75(1):28–36.

18. Mothershed EA, Whitney AM. Nucleic acid-based methods for the detection of bacterial pathogens: present and future considerations for the clinical laboratory. Clin Chim Acta. 2006;363(1–2):206–20.

19. Kondori N, Kurtovic A, Piñeiro-Iglesias B, Salvà-Serra F, Jaén-Luchoro D, Andersson B, et al. Mass spectrometry proteotyping-based detection and identification of Staphylococcus aureus, Escherichia coli, and Candida albicans in blood. Front Cell Infect Microbiol. 2021;11:634215.

20. Gill AA, Singh S, Thapliyal N, Karpoormath R. Nanomaterial-based optical and electrochemical techniques for detection of methicillin-resistant Staphylococcus aureus: a review. Microchim Acta. 2019;186:1–19.

21 da Silva ET, Souto DE, Barragan JT, Giarola JF, de Moraes AC, Kubota LT. Electrochemical biosensors in point-of-care devices: recent advances and future trends. ChemElectroChem. 2017;4(4):778–94.

22. Hernández-Rodríguez JF, Rojas D, Escarpa A. Electrochemical sensing directions for next-generation healthcare: trends, challenges, and frontiers. Anal Chem. 2020;93(1):167–83.

23. Campuzano S, Pedrero M, Yáñez-Sedeño P, Pingarrón JM. New challenges in point of care electrochemical detection of clinical biomarkers. Sens Actuators, B Chem. 2021;345:130349.

24. Corrigan D, Schulze H, Henihan G, Hardie A, Ciani I, Giraud G, et al. Development of a PCR-free electrochemical point of care test for clinical detection of methicillin resistant Staphylococcus aureus (MRSA). Analyst. 2013;138(22):6997–7005.

25 Yamanaka K, Vestergaard MdC, Tamiya E. Printable electrochemical biosensors: a focus on screen-printed electrodes and their application. Sensors. 2016;16(10):1761.

26. Alarcon B, Vicedo B, Aznar R. PCR-based procedures for detection and quantification of Staphylococcus aureus and their application in food. J Appl Microbiol. 2006;100(2):352–64.

27. Xie G, Zhou D, Zhao G, Feng X, Aguilar ZP, Xu H. Recombinase aided amplification with photoreactive DNA-binding dye for rapid detection of viable Staphylococcus aureus. Lwt. 2021;135:110249.

28. Yin W, Zhu L, Xu H, Tang Q, Ma Y, Chou S-H, He J. Bio-hybrid nanoarchitectonics of nanoflower-based ELISA method for the detection of Staphylococcus aureus. Sens Actuators, B Chem. 2022;366:132005.

29. Pineault K, Danis B, Lory S, Yuill D. Challenges in development and qualification of PCR/dPCR assays for gene therapy biodistribution and viral shedding assessment. J Appl Bioanal. 2023;9:e23003.

30. Peng P, Liu C, Li Z, Xue Z, Mao P, Hu J, et al. Emerging ELISA derived technologies for in vitro diagnostics. TrAC, Trends Anal Chem. 2022;152:116605.

31. Taleat Z, Khoshroo A, Mazloum-Ardakani M. Screen-printed electrodes for biosensing: a review (2008–2013). Microchim Acta. 2014;181(9):865–91.

32. Ghalkhani M, Sohouli E, Khaloo SS, Vaziri MH. Architecting of an aptasensor for the staphylococcus aureus analysis by modification of the screen-printed carbon electrode with aptamer/Ag–Cs-Gr QDs/NTiO2. Chemosphere. 2022;293:133597.

33. Xu C, Cheng S, Zhang F, Wang Q. Simultaneous detection of *Staphylococcus aureus* and E. coli O157:H7 using a self-calibrated potentiometric sensors array based on peptide recognition. IEEE Sensors J. 2023;23(15):17399–406. https://doi.org/10.1109/JSEN.2023.3285617.

34. Hashem A, Hossain MAM, Marlinda AR, Mamun MA, Simarani K, Johan MR. Nanomaterials based electrochemical nucleic acid biosensors for environmental monitoring: A review. Appl Surf Sci Adv. 2021;4:100064.

35. Shan X, Kuang D, Feng Q, Wu M, Yang J. A dual-mode ratiometric aptasensor for accurate detection of pathogenic bacteria based on recycling of DNAzyme activation. Food Chem. 2023;423:136287.

36. Wu YX, Kwon YJ. Aptamers: the "evolution" of SELEX. Methods. 2016;106:21–8.

37. Acquah C, Danquah MK, Yon JL, Sidhu A, Ongkudon CM. A review on immobilised aptamers for high throughput biomolecular detection and screening. Anal Chim Acta. 2015;888:10–8.

38. Muñoz J, Baeza M. Customized bio-functionalization of nanocomposite carbon paste electrodes for electrochemical sensing: a mini review. Electroanalysis. 2017;29(7):1660–9.

39. Soleimani S, Arkan E, Jalalvand AR, Goicoechea HC. Fabrication of a novel electrochemical aptasensor assisted by a novel computerized monitoring system for real-time determination of the prostate specific antigen: a computerized experimental method brought elegancy. Microchem J. 2020;157:104898.

40. Bai X, Wang Y, Song Z, Feng Y, Chen Y, Zhang D, Feng L. The basic properties of gold nanoparticles and their applications in tumor diagnosis and treatment. Int J Mol Sci. 2020;21(7):2480.

41. Hammami I, Alabdallah NM. Gold nanoparticles: synthesis properties and applications. J King Saud Univ Sci. 2021;33(7):101560.

42. Grel H, Ratajczak K, Jakiela S, Stobiecka M. Gated resonance energy transfer (gRET) controlled by programmed death protein ligand 1. Nanomaterials. 2020;10(8):1592.

43. Lakhera P, Chaudhary V, Jha A, Singh R, Kush P, Kumar P. Recent developments and fabrication of the different electrochemical biosensors based on modified screen printed and glassy carbon electrodes for the early diagnosis of diverse breast cancer biomarkers. Mater Today Chem. 2022;26:101129.

44. Eshlaghi SN, Syedmoradi L, Amini A, Omidfar K. A label-free electrochemical aptasensor based on screen printed carbon electrodes with gold nanoparticles-polypyrrole composite for detection of cardiac troponin I. IEEE Sens J. 2023;23(4):3439–45.

45. El-Wekil MM, Halby HM, Darweesh M, Ali ME, Ali R. An innovative dual recognition aptasensor for specific detection of Staphylococcus aureus based on Au/Fe3O4 binary hybrid. Sci Rep. 2022;12(1):12502.

46 Nguyen TT-Q, Kim ER, Gu MB. A new cognate aptamer pair-based sandwich-type electrochemical biosensor for sensitive detection of Staphylococcus aureus. Biosens Bioelectron. 2022;198:113835.

47. Tian J-Y, Liu X, Zhang S, Chen K, Zhu L, Song Y, et al. Novel aptasensing strategy for efficiently quantitative analyzing Staphylococcus aureus based on defective copper-based metal–organic framework. Food Chem. 2023;402:134357.

48. Sohouli E, Ghalkhani M, Zargar T, Joseph Y, Rahimi-Nasrabadi M, Ahmadi F, et al. A new electrochemical aptasensor based on gold/nitrogen-doped carbon nano-onions for the detection of Staphylococcus aureus. Electrochim Acta. 2022;403:139633.

49. Zhou H, Guo W, Wang S, Hao T, Wang Z, Hu Y, Wang S, Xie J, Jiang X, Guo Z. Ultrasensitive electrochemical aptasensor for *staphylococcus aureus* by stepwise signal amplification. https://doi.org/10.2139/ssrn.4066370.

50. Sabbih GO, Wijesinghe KM, Algama C, Dhakal S, Danquah MK. Computational generation and characterization of IsdA-binding aptamers with single-molecule FRET analysis. Biotechnol J. 2023;18:e2300076. https://doi.org/10.1002/biot.202300076.

51. Saeed AA, Abbas MN, Singh B, Abou-Zeid RE, Kamel S. Cellulose nanocrystals decorated with gold nanoparticles immobilizing GOx enzyme for non-invasive biosensing of human salivary glucose. Anal Methods. 2019;11(48):6073–83.

52. Upan J, Banet P, Aubert P-H, Ounnunkad K, Jakmunee J. Sequential injection-differential pulse voltammetric immunosensor for hepatitis B surface antigen using the modified screen-printed carbon electrode. Electrochim Acta. 2020;349:136335.

53. Fischer MJE. Amine coupling through EDC/NHS: a practical approach. In: Mol N, Fischer M, editors. Surface plasmon resonance. Methods in Molecular Biology, vol 627. Humana Press; 2010. https://doi.org/10.1007/978-1-60761-670-2_3.

54. Raghav R, Srivastava S. Immobilization strategy for enhancing sensitivity of immunosensors: L-Asparagine–AuNPs as a promising alternative of EDC–NHS activated citrate–AuNPs for antibody immobilization. Biosens Bioelectron. 2016;78:396–403.

55. Naghshbandi B, Adabi M, Pooshang Bagheri K, Tavakolipour H. Design of a new electrochemical aptasensor based on screen printed carbon electrode modified with gold nanoparticles for the detection of fumonisin B1 in maize flour. J Nanobiotechnol. 2022;20(1):534.

56. Mokwebo KV, Oluwafemi OS, Arotiba OA. An electrochemical cholesterol biosensor based on a CdTe/CdSe/ZnSe quantum dots—poly (propylene imine) dendrimer nanocomposite immobilisation layer. Sensors. 2018;18(10):3368.

57. Singh M, Sahoo A, Yadav K, Sharma Y. Toward the origin of magnetic field-dependent storage properties: a case study on the supercapacitive performance of FeCo2O4 nanofibers. ACS Appl Mater Interfaces. 2020;12(44):49530–40.

58. Venton BJ, DiScenza DJ. Voltammetry. Electrochem Bioanalysis. 2020;27–50. https://doi.org/10.1016/B978-0-12-821203-5.00004-X.

59. Deffo G, Nde Tene TF, Medonbou Dongmo L, Zambou Jiokeng SL, Tonleu Temgoua RC. Differential pulse and square-wave voltammetry as sensitive methods for electroanalysis applications. In: Wandelt K, Bussetti G, editors. Encyclopedia of Solid-Liquid Interfaces. 1st ed. Oxford: Elsevier; 2024. p. 409–17.

60. Lichtman JW, Conchello J-A. Fluorescence microscopy. Nat Methods. 2005;2(12):910–9.

61. Akhtar K, Khan SA, Khan SB, Asiri AM. Scanning electron microscopy: principle and applications in nanomaterials characterization. In: Sharma S, editor. Handbook of materials characterization. Cham: Springer; 2018. https://doi.org/10.1007/978-3-319-92955-2_4.

62. Chandra P, Noh H-B, Won M-S, Shim Y-B. Detection of daunomycin using phosphatidylserine and aptamer co-immobilized on Au nanoparticles deposited conducting polymer. Biosens Bioelectron. 2011;26(11):4442–9.

63. Zhang X, Yadavalli VK. Surface immobilization of DNA aptamers for biosensing and protein interaction analysis. Biosens Bioelectron. 2011;26(7):3142–7.

64. Oberhaus FV, Frense D, Beckmann D. Immobilization techniques for aptamers on gold electrodes for the electrochemical detection of proteins: a review. Biosensors. 2020;10(5):45.

65. Ahmad HM, Andrade A, Song E. Continuous real-time detection of serotonin using an aptamer-based electrochemical biosensor. Biosensors. 2023;13(11):983.

66. Settu K, Liu J-T, Chen C-J, Tsai J-Z. Development of carbon–graphene-based aptamer biosensor for EN2 protein detection. Anal Biochem. 2017;534:99–107.

67. Maeno H, Wong P-F, AbuBakar S, Yang M, Sam S-S, Jamil-Abd J, et al. A 3D Microfluidic ELISA for the detection of severe dengue: sensitivity improvement and vroman effect amelioration by EDC–NHS surface modification. Micromachines. 2021;12(12):1503.

68. Ning K, Shen Y, Yao Y, Xie W, Ma C, Xu Q. Aptamer–molecularly imprinted polymer multiple-recognition system: construction and application. Chemosensors. 2023;11(8):465.

69. Yunus MH, Yusof NA, Ismail S, Md Noor SS, Mohammad F, Sulaiman Y, et al. Surface-enhanced carboxyphenyl diazonium functionalized screen-printed carbon electrode for the screening of tuberculosis in sputum samples. Nanomaterials. 2022;12(15):2551.

70. Sabbih GO, Wijesinghe KM, Algama C, Dhakal S, Danquah MK. Computational generation and characterization of IsdA-binding aptamers with single-molecule FRET analysis. Biotechnol J. 2023;18(12):2300076.

71. Sari AK, Hartati YW, Gaffar S. A review on the development of aptamer immobilization techniques in aptamer-based electrochemical biosensors for viruses detection. Anal Bioanal Electrochem. 2022;14(1):127–43.

72. Dauphin-Ducharme P, Churcher ZR, Shoara AA, Rahbarimehr E, Slavkovic S, Fontaine N, et al. Redox reporter-ligand competition to support signaling in the cocaine-binding electrochemical aptamer-based biosensor. Chemistry–A Eur J. 2023;29(35):202300618.

73. Thevendran R, Citartan M. Assays to estimate the binding affinity of aptamers. Talanta. 2022;238:122971.

74. Li H-H, Wen C-Y, Hong C-Y, Lai J-C. Evaluation of aptamer specificity with or without primers using clinical samples for C-reactive protein by magnetic-assisted rapid aptamer selection. RSC Adv. 2017;7(68):42856–65.

75. Mohamad T. Limit of blank (LOB), limit of detection (lOD), and limit of quantification (LOQ). Org Med Chem Int J. 2018;7(5):555722. https://doi.org/10.19080/OMCIJ.2018.07.555722.

76. Montville D, Voigtman E. Statistical properties of limit of detection test statistics. Talanta. 2003;59(3):461–76.